

Provided for non-commercial research and education use.
Not for reproduction, distribution or commercial use.



This article appeared in a journal published by Elsevier. The attached copy is furnished to the author for internal non-commercial research and education use, including for instruction at the authors institution and sharing with colleagues.

Other uses, including reproduction and distribution, or selling or licensing copies, or posting to personal, institutional or third party websites are prohibited.

In most cases authors are permitted to post their version of the article (e.g. in Word or Tex form) to their personal website or institutional repository. Authors requiring further information regarding Elsevier's archiving and manuscript policies are encouraged to visit:

<http://www.elsevier.com/copyright>



Contents lists available at ScienceDirect

Planetary and Space Science

journal homepage: www.elsevier.com/locate/pss

High Lake gossan deposit: An Arctic analogue for ancient Martian surficial processes?

L. West^a, D.J. McGown^a, T.C. Onstott^{a,*}, R.V. Morris^b, P. Suchecky^c, L.M. Pratt^c

^a Department of Geosciences, Princeton University, Princeton, NJ 08544, USA

^b ARES, NASA Johnson Space Center, Houston, TX, USA

^c Department of Geological Sciences, Indiana University, Bloomington, IN, USA

ARTICLE INFO

Article history:

Received 24 December 2008

Received in revised form

13 May 2009

Accepted 18 May 2009

Available online 3 June 2009

Keywords:

Mars analogue

Mineralogy

Gossan

Arctic

Mössbauer

ABSTRACT

Gossan samples collected during a reconnaissance expedition to High Lake in Nunavut, Canada, were analyzed to determine their mineral components and to define parameters for the geochemical environment in which they formed. The gossan represents a natural acid drainage site in an arctic environment that serves as an analogue to the conditions under which sulfate and Fe-oxide possibly formed on Mars. Rock and soil samples were taken from three different outcrops and analyzed using XRD, SEM/EDS and Mössbauer. Two main mineral assemblages were observed. The first assemblage, which was found primarily in samples from the first outcrop, contained chlorite, Fe-phosphates, Fe-oxide and quartz. The second assemblage, which was found at the second and third outcrops, was primarily quartz, mica and jarosite. One sample (G41), containing Fe-oxide, jarosite and gypsum, appears to be transitional between a Fe-oxide dominant assemblage to a jarosite dominant assemblage. Thermodynamic equilibria predicts that the gossan pore water should range from mildly acidic, relatively sulfate-poor (pH 3–6; $\text{SO}_4 < 1000 \text{ mg l}^{-1}$) to highly acidic and relatively sulfate-rich (pH 0.5–3; $\text{SO}_4 > 3000 \text{ mg l}^{-1}$) for the first and second mineral assemblages, respectively. Kinetic reaction models indicate that the second assemblage replaces the first during evaporation or freezing of water. Compared to acid mine drainage (AMD) sites located in temperate regions, the arctic High Lake gossan lacks diversity in sulfate species and has smaller diagenetic crystal sizes. The smaller crystal size may reflect the slower reaction rates at colder temperatures and the seasonal water saturation. These initial results indicate that the High Lake gossan deposit does record mechanisms for which minerals like hematite, goethite, gypsum and jarosite, which are found on Mars, can form in an environment that involves seasonal water occurrence in a cold climate.

© 2009 Elsevier Ltd. All rights reserved.

1. Introduction

Beginning with the chemical analyses by the Viking landers (e.g., Clark et al., 1976; Clark, 1993), scientists hypothesized that sulfates are present on the Martian surface on the basis of SO_3 concentrations (~6–9%) and that sulfate was compatible with the oxidizing environment implied by the pervasive Fe-oxides. Opportunity's Mössbauer (MB) instrument detected the presence of the sulfate-bearing mineral, jarosite [(K, Na, H_3O) (Fe, Al)₃ (SO_4)₂(OH)₆] (Klingelhöfer et al., 2004; Morris et al., 2006), and the rover's microscopic imager detected "vugs" in the sedimentary layering with the shape of gypsum crystals. The alpha particle X-ray spectrometer (APXS) determined that the rock strata contained up to ~25% SO_3 (Rieder et al., 2004). The strata also contained spherical nodules composed of hematite [Fe_2O_3]

(millimeters to centimeters in diameter) found as concretions within the sedimentary layering of the crater wall and scattered about the surface due to erosion (Catling, 2004). These lines of evidence were interpreted as indicating the deposition of sulfate minerals in an acidic, aqueous environment (Squyres et al., 2004). Layered deposits comprised of sulfate minerals have since been mapped from orbit by OMEGA in Valles Marineris (Bibring et al., 2005) and in the northern polar region (Langevin et al., 2005).

Although different theories exist for the origin of sulfates on Mars, the major depositional environments for jarosite, gypsum and Fe-oxyhydroxides on Earth suggest an acidic and oxidizing aqueous environment. Jarosite is most commonly found associated with sulfide mines across the world. K-Jarosite is found to precipitate from water with pH less than ~3, high Fe^{3+} and SO_4^{2-} concentrations and high K/Na ratios (Jamieson et al., 2004) and possibly requires increased temperatures for extended periods of time (Majzlan and Myeni, 2005). Hydronium jarosite is found as an evaporite mineral at the Rio Tinto in Spain (Fernandez-Remolar et al., 2003; Fernandez-Remolar et al., 2005), which has been

* Corresponding author. Tel.: +1 609 258 7678.

E-mail address: tullis@princeton.edu (T.C. Onstott).

contaminated by an abandoned, 5000 year old Cu, Au and Ag mine (Salkield, 1987).

Currently, three models are proposed for the origin of the jarosite/hematite mineral assemblage at Meridiani Planum. The first is that between 3.9 and 3.5 billion years ago (Ga) during the Naochian Epoch a briny, oxidizing, acidic, playa environment existed on the Martian surface (Grotzinger et al., 2005; McLennan et al., 2005). The second proposes that the deposits were created by impact derived base surge flows (Knauth et al., 2005). The third proposes that the deposits result from a fumarolic alteration of basaltic volcanic deposits (McCullom and Hynek, 2005). Absent from the latter two models is the requirement for near-surface water that would provide the best prospects for surface life on ancient Mars.

The argument for the Naochian playa environment is drawn largely from discoveries by *Opportunity*. Its images show centimeter scale cross-bedding and penecontemporaneous joints that crosscut lamination. Grotzinger et al. (2006) interpreted the cross-bedding as cross lamination, a fluvial process differing fundamentally in geometry and scale from cross-bedding due to impact driven base surge deposits. The joints, Grotzinger et al. (2006) contended, are dehydration artifacts. McLennan et al. (2005) interpreted the recrystallization and secondary porosity within specific stratigraphic layers, the hematitic concretions, the gypsum-shaped vugs and other evidence for synsedimentary deformation such as contorted bedding as having resulted from the evaporation of acidic waters followed by multiple episodes of cementation and alteration during interaction with groundwater.

Knauth et al. (2005) argue that the acidic, playa environment is unlikely because acidic solutions would quickly neutralize and precipitate clay minerals which were not detected by *Opportunity*. Their impact theory proposes that Ca- and Mg-sulfate crystallized from pre-existing brine and that the impact later ejected these sulfates and transported them along with other salts and brine-soaked, sulfide-bearing, basaltic debris to the surface as massive base surges. With exposure to surface conditions, the materials weathered into acidic sulfates such as jarosite (Burt et al., 2006).

The fumarolic theory advanced by McCullom and Hynek (2005) is based upon their observation that with the exception of sulfur, the cation to Si+Al ratios in Meridiani bedrocks are almost identical to basalts found in the Martian meteorite Shergotty. The problem with the sulfur is that enrichment by evaporation should produce proportional increases in cations to balance any precipitating sulfates, but none are observed. To explain this discrepancy, McCullom and Hynek (2005) proposed that the sedimentary strata actually represent basaltic pyroclastic deposits, which can have sedimentary depositional features, and that they were altered by the condensation of fumarolic vapors rich in SO₂ and H₂O. The Fe²⁺ released in the Fe-bearing silicates is oxidized then by atmospheric O₂. As this condensed water evaporates, sulfate was formed. Because hematite spherules require higher temperatures, these most likely formed after the rocks were already altered but still warm (>100 °C) (McCullom and Hynek, 2005).

Terrestrial analogues and laboratory experiments provide supportive evidence for the fumarolic (hydrothermal) alteration hypothesis. Mineral assemblages including jarosite, alunite [KAl₃(SO₄)₂(OH)₆], silica, pyrite [FeS₂], gypsum and barite [BaSO₄] are found in active, andesitic stratovolcanoes such as Mt. Hood, Mt. Rainier and Shasta in the Cascade Range (Zimbelman et al., 2004) and at basaltic Kilauea volcano in Hawaii (Schiffman et al., 2006) on Hawaii. These minerals formed when the original bedrock is altered by an acid fog. At Kilauea, SO₂ emitted from the crater condenses into H₂SO₄-rich aerosols which are carried away by local winds. As the fog is transported away, the aerosols cool and precipitate over a ~20 km² area of tephra. With

evaporation, the S-rich aerosols react with the tephra to form thin, amorphous silica and jarosite coatings (Schiffman et al., 2006). In addition, some jarosite group minerals and smectitic clay formed from supergene oxidation of hydrothermal pyrite (Zimbelman et al., 2004). At Mauna Kea volcano (Hawaii), sulfate-rich phases (jarosite and alunite) and hematite spherules result from hydrothermal alteration of basaltic tephra by acid-sulfate vapors and solutions (Morris et al., 2005). Experiments by Golden et al. (Golden et al., 2008) demonstrated that hydronium jarosite and hematite spherules can form from acid-sulfate solutions under hydrothermal conditions. The question remains as to whether hematite and more specifically hematite spherules, can form at low temperatures or are only produced at high temperatures.

This report focuses on the mineral assemblages associated with a high arctic gossan on the High Lake mining property in the Nunavut province, Canada. Gossans, on Earth, are formed where sulfide ore deposits are oxidized in flowing or standing water resulting in acid that leaches soluble ions from the host rock producing hydrated Fe-oxides and sulfates that bear a superficial resemblance to Martian regolith (Burns, 1988; Burt et al., 2006). The gossan outcrops at High Lake occur on Archean-age, massive, volcanogenic sulfide deposits and their reddish-orange color and complete lack of vegetation make them readily visible in satellite images of High Lake (Fig. 1A). Although the permafrost at High Lake is ~440 m thick (Piffner et al., 2008), drilling indicates that the gossan under study only extends to a depth of ~1 m, and is thus confined to the seasonally frozen, active layer. Additionally, glacial scouring implies that any previous fractured, surface gossan was likely removed during glaciation. Thus, this gossan is presumed to have formed within the last several thousands of years since deglaciation of this region. The goal of this paper is to examine this environment for evidence of mineral assemblages similar to those reported at Terra Meridiani by *Opportunity*. This site also provides a natural laboratory for examination of the effects of temperature, water availability and *f*O₂ on the oxidation rates of sulfide, the formation rates of sulfate and oxide mineral assemblages and the microbial activities associated with each.

2. Procedures

2.1. Field methods

The High Lake mining property (67°22'47"N, 110°50'37"W) is located within a 2.7 Ga, green schist facies, felsic and mafic metavolcanic belt with a significant Cu–Zn sulfide deposit (Petch, 2005). The deposit was originally discovered in the 1950s by recognition of the km-scale gossans. A total of 43 samples, G1–G43, were collected from three different gossan locations at High Lake (Fig. 1A). Sample site #1, represented by samples G1–30, was located northwest of the mining camp in the A–B zone of the volcanogenic massive sulfide deposit (Petch, 2005). The rocks found in outcrop here and in the alluvial fan running northeast from the gossan towards High Lake are primarily quartz–chlorite–sulfide-bearing felsic metavolcanic rocks. Sample site #2, represented by samples G31–33, was located at the northern end of the D sulfide pod and occurs on a small plateau between the main drill site HLW-03-28 and the small lake to its east (Fig. 1A). The cores from this area indicate that the surface rock is composed of felsic metavolcanic with some dioritic intrusions. Sample site #3 (Fig. 1A and B), represented by samples G34–43, was located at the E zone sulfide exposed on the southern shore of the same small lake. The cores taken at this outcrop indicated that the sulfide layers are associated with a mafic sill. The sulfides present in the zones are comprised

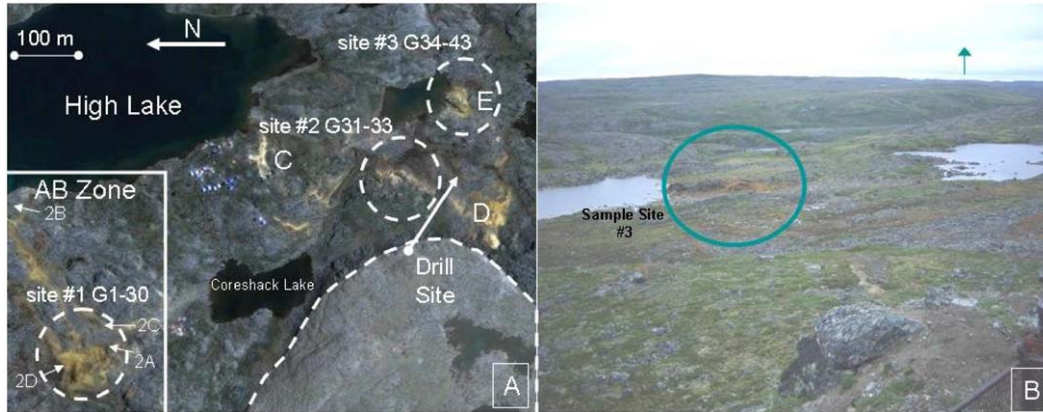


Fig. 1. (A) Satellite image of High Lake mining camp and gossan (courtesy of Google.com). Circles identify location of gossan samples collected in July 2007 and sample numbers for each location are indicated. The High Lake borehole was described in Pffiffer et al. (2008). Ore zones A–E are located in Petch (2005). 2A–2D are the locations of the photos shown in Fig. 2. The dashed white line demarcates the boundary between the metavolcanic strata to the east and the 2.6 Ga, granodiorite pluton to the west. (B) Aerial photograph of site #3.

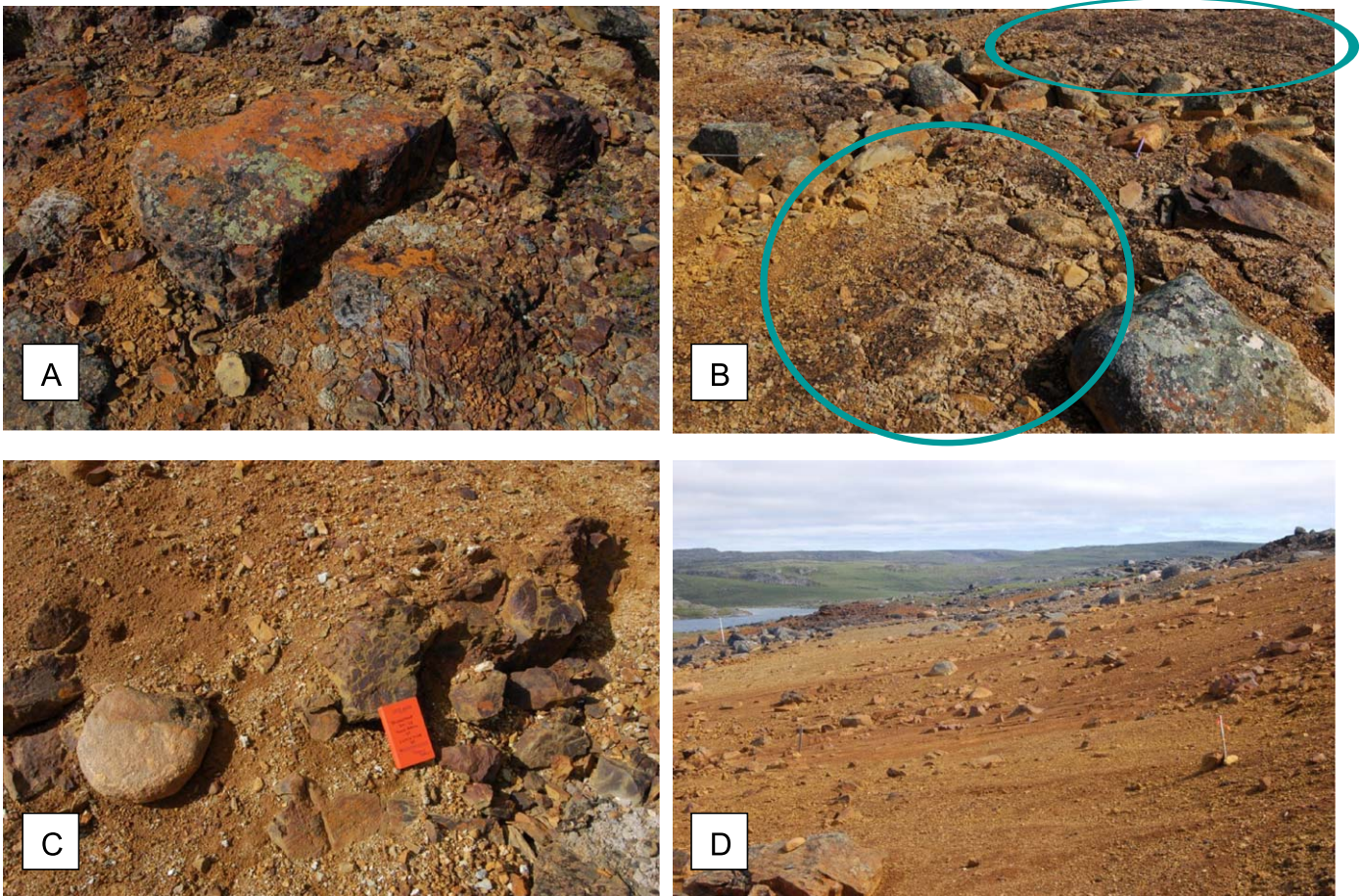


Fig. 2. (A) Gossan outcrop of mafic metavolcanic exhibiting lichen covered fracture surfaces and oxidized Fe coating. Photo taken near the top portion of the A–B zone. (B) Fungal apron forming on gossan regolith (circled). Photo taken at the lower southern edge of the A–B zone, ~10 m from High Lake. (C) Glacial colluvium draped over fractured gossan outcrop. Photo taken at the southern edge of A–B zone just past the upper part of the core yard. (D) Alluvial fan deposit down gradient from topographically highest gossan outcrops. View across the top of the A–B zone taken from the north, looking south. The southern end of High Lake is in the background.

primarily of chalcopyrite, pyrrhotite, sphalerite and pyrite (Petch, 2005). Each gossan site is comprised of intensely fractured bedrock or fractured glacial deposits covered with Fe-oxide coatings and lichen (Fig. 2A and C) forming a local topographic high surrounded by an apron of colluviums that extends outward to an alluvial plain devoid of vegetation (Fig. 2D). As the slope

diminishes the surface of the alluvial plain becomes bound by a several millimeter-thick fungal apron (Fig. 2B) that fringes the gossans.

For each gossan sample, ~100 g were collected in Falcon tubes and kept frozen for transport to Princeton University. Of the 43 samples, 23 were selected for analyses based upon their degree of

alteration with altered rock fragments being preferred. For analysis, 2–3 g of each sample was ground to a powder using ceramic mortar and pestle and kept refrigerated until analysis. Sample handling equipment was thoroughly cleaned between samples to minimize cross contamination.

2.2. XRD methods

The 23 powder samples were first analyzed using a Rigaku Miniflex X-ray diffractometer (XRD) using Cu K α 1 radiation. The powder was placed onto a glass slide and acetone was used to suspend the powder so that it was randomly and evenly distributed over the slide. After acetone evaporation, the slide was placed on a steel sample holder and attached to a magnetic stage of the XRD. The XRD was scanned from 5 to 90 °C in 0.04° steps with each run lasting approximately 1½ h. All powder XRD spectra were analyzed using the JADE 3.1 software package. The software was used to correct for increasing X-ray fluorescence from Fe with increasing 2 θ to more easily discern the less intense peaks. A combination of the JCPDS mineral search manual book and the online database from Mincrust was utilized to identify the mineral corresponding to each peak in the XRD spectrum.

2.3. SEM/EDS methods

Based upon the XRD results, a sample suite that represented the full range of mineral assemblages was selected for SEM/EDS and Mossbauer analyses. Samples G2, G8, G9 and G10 from site 1, sample G33 from site 2, and samples G40, G41 and G43 from the third site were chosen. Preparation for the SEM involved using the same starting material used for the XRD. The samples were sprinkled on to double-sided carbon tape attached to separate 1 in SEM stubs. After removing loose material, the samples were carbon-coated to prevent charging. The eight samples were analyzed by a Phillips XL30 FEG SEM with a Princeton Gammatech

EDS. The EDS instrumentation and software collected data and ran compositional analyses, while the beam was scanned across the sample to obtain a bulk composition and from selected spots on specific minerals. The combination of imaging and elemental analyses allowed for the identification and confirmation of mineral identification by XRD. The SEM enabled location and identification of minerals that were either amorphous, to small (nm scale), or present in too minute a quantity (<1%) to have a distinct effect on the XRD patterns. The SEM also enabled the textural relationships between the different phases to be delineated. The spectrum and quantification reports for EDS were not exact values and were subject to considerable error. Therefore, they were not taken as representative of the actual atomic composition of the minerals but were used as relative values indicating the general composition of a mineral.

2.4. Mössbauer methods

Transmission Mössbauer measurements at ~293 K were made at the NASA Johnson Space Center on Ranger Scientific spectrometers (Morris et al., 2000). Absorbers were made by dispersing the samples in epoxy. The Mössbauer parameters, derived by fitting folded spectra to theoretical line shapes using an in-house computer program (JSCFIT), were the isomer shift, δ , relative to metallic Fe foil at 293 K, the quadrupole splitting, ΔEQ , the hyperfine field strength, B_{hf} , the full-width at half-maximum intensity, Γ , and the percentage of total Fe associated with each subspectral component, A. For the fitting procedure, the two peaks in doublet subspectra were constrained to have equal areas and widths. In sextet subspectra, the peak areas in sextet subspectra were constrained to the ratio 3:2:1:1:2:3, and peaks with equal intensities were constrained to have equal widths. The mineralogical assignments of subspectral components are based on literature (Burns and Solberg, 1990; McCammon, 1995; Stevens et al., 1998) and in-house compilations of Mössbauer parameters.

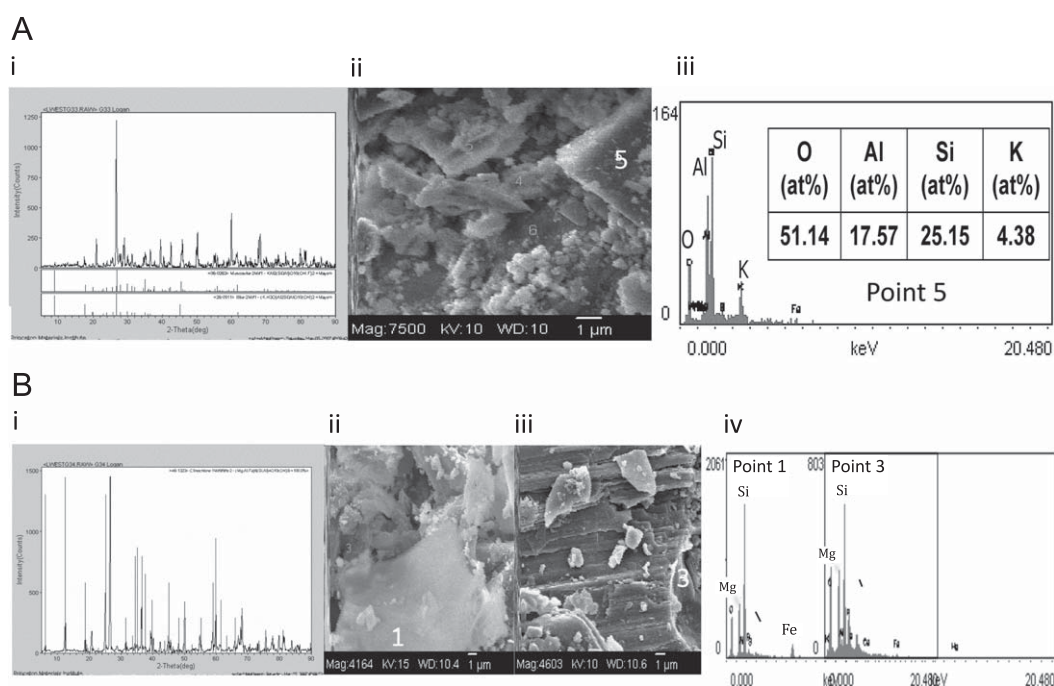


Fig. 3. (A) Muscovite, Illite: (i) representative XRD pattern match for illite and muscovite from sample G33; (ii) SEM image and (iii) EDS results for an amiac crystal sheet from sample G10. The platy morphology and high Al values are typical of mica such as muscovite or illite. (B) (i) representative XRD pattern matches for clinocllore from G34. SEM image and EDS results for a platy Mg-silicate from sample G8 (ii and iv) and for a tabular Mg-silicate from sample G43 (iii and iv). These are most likely chlorites such as clinocllore and chamosite or amesite or corrensite.

2.5. Geochemical modeling

The mineral assemblages were used to derive the pore water chemistry by using the ACT2 code and the SEM diagenetic relationships were modeled using the REACT code of Geochemist Workbench, version 7.04 (Rockware, Inc., Golden, CO) (Bethke, 1998).

3. Results

3.1. XRD and SEM/EDS results

The most dominant mineral species, identifiable by XRD in 22 of the 23 samples analyzed, was quartz. Sample G5 from site #1 was essentially pure quartz (Fig. 3A). In every SEM analysis, the largest grains (~250 μm) were composed of quartz coated by surface mineral precipitates (Fig. 3A).

Muscovite [KAl₂Si₃AlO₁₀(OH)₂] was detected in four samples (G9, G10, G33 and G40; Table 1), and illite [(K,H₃O)Al₂Si₃AlO₁₀(OH)₂] was detected in two samples (G10 and G33). SEM images depicted these Al-silicates as thin, platy minerals with significant K and Al peaks in the EDS analyses (Fig. 3B). The other phyllosilicates that were detected by XRD belonged to the chlorite or kaolinite–serpentine groups, including amesite [(Mg, Al)₃SiAlO₅(OH)₄] in G8, corrensite [(Mg, Al)₉(Si, Al)₈O₂₀(OH)₁₀·4H₂O] in G2, G8 and G9, talc [Mg₃Si₄O₁₀(OH)₂] in G2 and G8, chamosite [(Fe, Al, Mg, Mn)₆(Si, Al)₄O₁₀(OH)₈] in G2, G8, G9 and G43, and clinocllore [(Mg, Al)₆(Si, Al)₄O₁₀(OH)₈] in G2, G8 and G9 (Table 1). Either chamosite or clinocllore were present in 16 of the 23 samples. In SEM images Mg-silicates appeared either as tabular crystals ranging between 4 and 200 μm or as μm-size platelets (Fig. 3C). The most prominent amphibole detected in the XRD spectra was magnesioanthophyllite [Mg₇Si₈O₂₂(OH)₂], which was present in both site #1 and #3, in samples G9 and G41.

Aside from silicates, phosphate minerals commonly occurred as foggite [CaAl(PO₄)(OH)₂·2H₂O] and augelite [Al₂(PO₄)(OH)₃] based on XRD data (Table 1). At least one of these two was present in samples G2, G8, G9 and G10 from site #1. In SEM images phosphates generally appeared as small (<1 μm) amorphous to sub-rounded crystals resting on larger crystals (Fig. 4A).

On the basis of XRD data, oxides commonly occurred as hematite and/or goethite from site #1 (G2, G8 and G9 in Fig. 4B) and both were absent from the less altered samples. Although hematite and goethite were not identified by XRD for sample 41, SEM and EDS analyses revealed Fe-oxide coatings were present in minor abundance (Fig. 4B). The small-particle (≤10 nm), poorly crystalline phases ferrihydrite and schwertmannite [Fe₁₆O₁₆(OH)₂(SO₄)₂] are identified by their broad powder diffraction peaks between 50° and 55° 2θ (sample G2) and 33° and 40° 2θ (sample G2) (Fig. 4B), respectively (Murad and Rojik, 2005). SEM images of G41 revealed several different morphologies for Fe-oxides ranging from ~0.5 μm, subhedral grains to small, amorphous to rounded precipitates (Fig. 4B), but schwertmannite was not confirmed by SEM/EDS analyses. Mn-oxide minerals were also detected in some samples as groutite [MnO(OH)] at site #1 (G2) and as pyrochroite [Mn(OH)₂] at site #3 (G43).

The only other commonly occurring mineral group was the sulfates. These included the Fe-bearing sulfates, jarosite, natrojarosite [NaFe³⁺(SO₄)₂(OH)₆] and rhomboclase [(H₅O₂)⁺Fe³⁺(SO₄)₂·2(H₂O)] (Fig. 4C). Samples G2, G10, G33, G40, G41 and G43 contained one of these three sulfates. Gypsum was also detected, but only in G41 by both XRD and SEM-EDS as μm-size platelets; anhydrite was not detected. Although rhomboclase was not located in any SEM images, gypsum and jarosite were represented by 1–5 μm, well-crystallized minerals (Fig. 4C).

Table 1
Minerals identified by XRD.

Sample	G2	G8	G9	G10	G33	G40	G43	G41
Sample site	1	1	1	1	2	3	3	3
Group	A	A	A	B	B	B	B	C
Silicates								
Quartz	X	X	X	X	X	X	X	X
Talc	X	X						
Spinel							X	
Mg-Anthophyllite			X					X
Chamosite	X	X	X				X	
Clinocllore	X	X	X					
Corrensite	X	X	X					
Microcline			X					
Nepheline					X			
Orthoclase			X					
Phlogopite			X				X	
Lepidolite				X	X			
Muscovite			X	X	X	X		
Illite				X	X			
Pyrophyllite			X					X
Amesite		X						
Kellyite		X						
Brindleyite		X						
Laumontite	X							
Stilbite		X						
Gismondine		X						X
Kaliophilite	X							
Cebollite				X				
Phosphates								
Augelite	X							
Foggite	X	X	X	X				
Hentschelite			X					
Lazulite			X					
Triplite				X				
Trolleite					X			
Woodhouseite								X
Oxides								
Ferrihydrite	X	X						X
Goethite	X	X	X					
Hematite	X							
Groutite	X							
Pyrochroite							X	
Sulfates								
Hydroniumjarosite				X				
Jarosite					X	X		X
Natrojarosite				X			X	
Gypsum								X
Rhomboclase	X							X
Schwertmannite	X							
Yavapaiite				X				

Of the eight samples examined using SEM/EDS and XRD analysis, seven are divisible into two groups having distinct mineral assemblages (Table 1). The Group A (G2, G8, G9) is physically described as dark red to rusty colored material and had elevated background in the XRD spectra consistent with their high Fe content. Scanned and spot EDS analyses indicate that most of this Fe was precipitated as Fe-oxides as there was a lack in other potential mineral anions such as Cl, SO₄²⁻ or CO₃²⁻ and a lack of Si correlated with Fe. The main assemblage of this group consisted of Fe-oxides, quartz, chlorite and phosphate minerals. Goethite, ferrihydrite and augelite were the important Fe-bearing minerals in these samples. Other phosphate minerals included lazulite [Mg, Fe²⁺Al₂(OH,PO₄)₂] and hentschelite [CuFe³⁺(OH, PO₄)₂].

Group B (G10, G33, G40 and G43) possessed colors ranging from green to tan to yellow-orange. The main minerals in these samples are muscovite, quartz and jarosite. The XRD spectra for these samples contained fewer mineral matches than the first

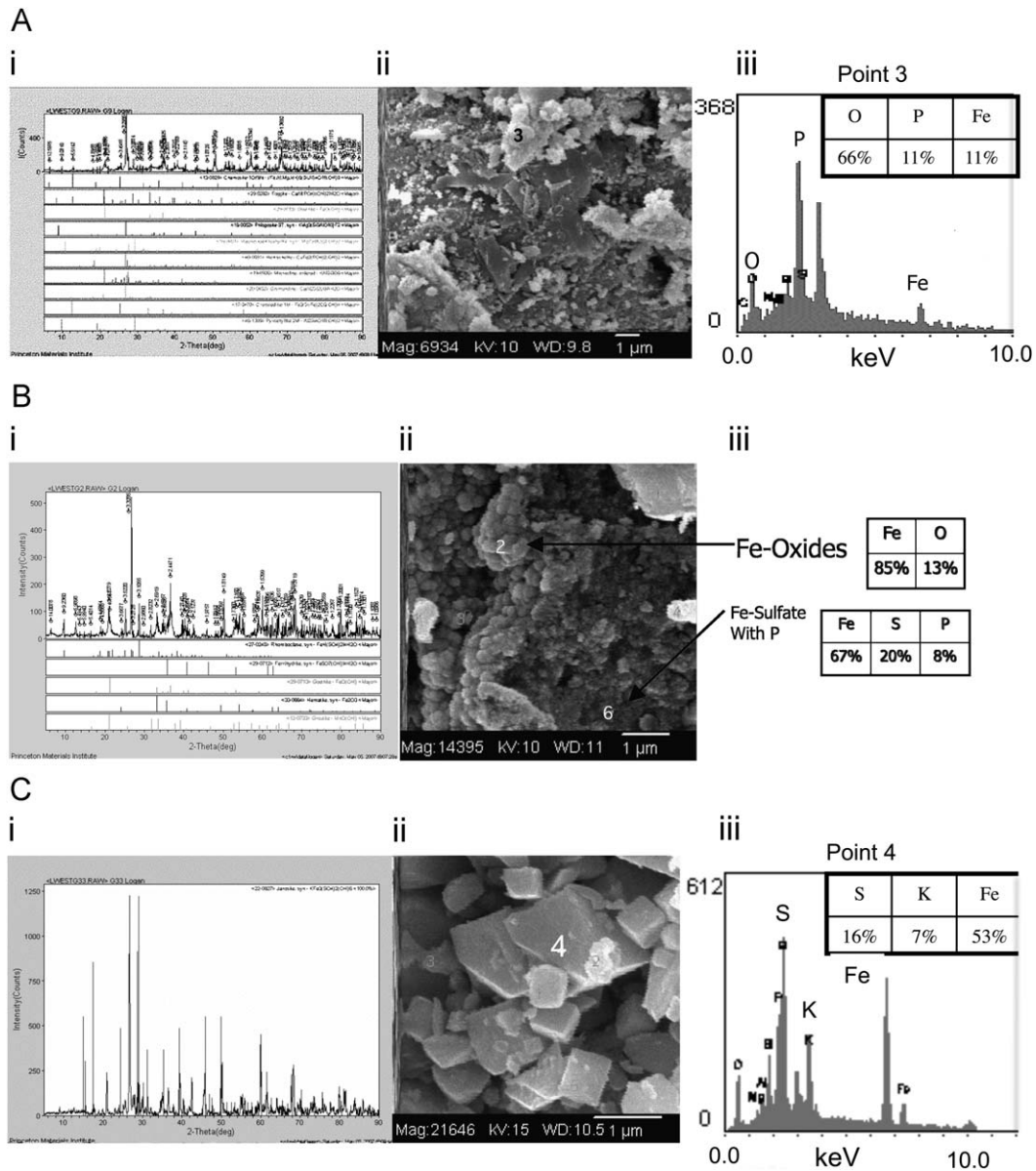


Fig. 4. (A) (i) XRD pattern for G9 containing three different phosphates; (ii) SEM image and (iii) EDS results for a Fe-phosphate from sample G9. Most phosphates identified by SEM were Fe-phosphates precipitated as small ($< 1 \mu\text{m}$) amorphous to sub-rounded crystals resting on larger crystals. (B) (i) Representative XRD pattern match for Fe-oxides from G2; (ii) SEM image and (iii) EDS results for a Fe-oxide from sample G41. C. (i) Representative XRD pattern match for jarosite from G33; SEM image and EDS result for jarosite in samples G33 (ii and iv) and G41 (iii). The cubic morphology is typical of jarosite and natrojarosite.

group. SEM/EDS analysis also detected Mg-silicates and P- and S-bearing mineral coatings. Scanning EDS analyses revealed a weak correlation between P and S with Fe or other cation amounts, but often not sufficient to electrically balance the S and P. The mineral phase(s) responsible for the coatings could not be identified by SEM/EDS, but XRD spectra detected the yellowish, Al phosphate mineral, Trolleite $[\text{Al}_4(\text{OH})(\text{PO}_4)_3]$, the brownish Mn- and Fe-phosphate mineral, triplite $[\text{Mn}^{2+}, \text{Fe}^{2+}]_2(\text{F},\text{OH})\text{PO}_4$ and the Fe^{3+} sulfate mineral, yavapaiite $[\text{KFe}(\text{SO}_4)_2]$.

G41 is unique from Groups A and B in that it is characterized by lower quartz abundance and by the only occurrence of gypsum ($\text{Ca}_2\text{SO}_4 \cdot 2\text{H}_2\text{O}$). The P and S in the sample were commonly associated with Fe or Ca, but high levels of Fe did not necessarily correlate with higher P and S values. XRD detected the presence of the phosphate mineral, woodhouseite $[\text{CaAl}_3((\text{OH})_6, \text{SO}_4, \text{PO}_4)]$.

3.2. Mössbauer analyses

Six samples were analyzed by MB: G2, G8 and G9 from Group A, G10 and G33 from Group B, and G41 from Group C (Fig. 5). The Mössbauer parameters calculated from least squares fits of the spectra are summarized in Table 2. The spectra were modeled by five Fe-bearing phases (Table 2): octahedrally coordinated Fe^{3+} (oct- Fe^{3+}) in nanophase ferric oxide (npOx); doublet subspectrum); oct- Fe^{3+} in jarosite (doublet subspectrum); oct- Fe^{2+} in an unassigned phase (doublet subspectrum), oct- Fe^{3+} in hematite (sextet subspectrum) and a Fe-bearing component that is represented by a singlet with a large peak width (Table 2). The broad singlet approximates contributions from partially relaxed sextets resulting from small particles and/or substitutional impurities (e.g., Al^{3+} for Fe^{3+}) in Fe-bearing oxides like hematite, magnetite, maghemite and goethite. The presence of poorly resolved peaks at high velocity (e.g., near -7.5 mm s^{-1} in sample

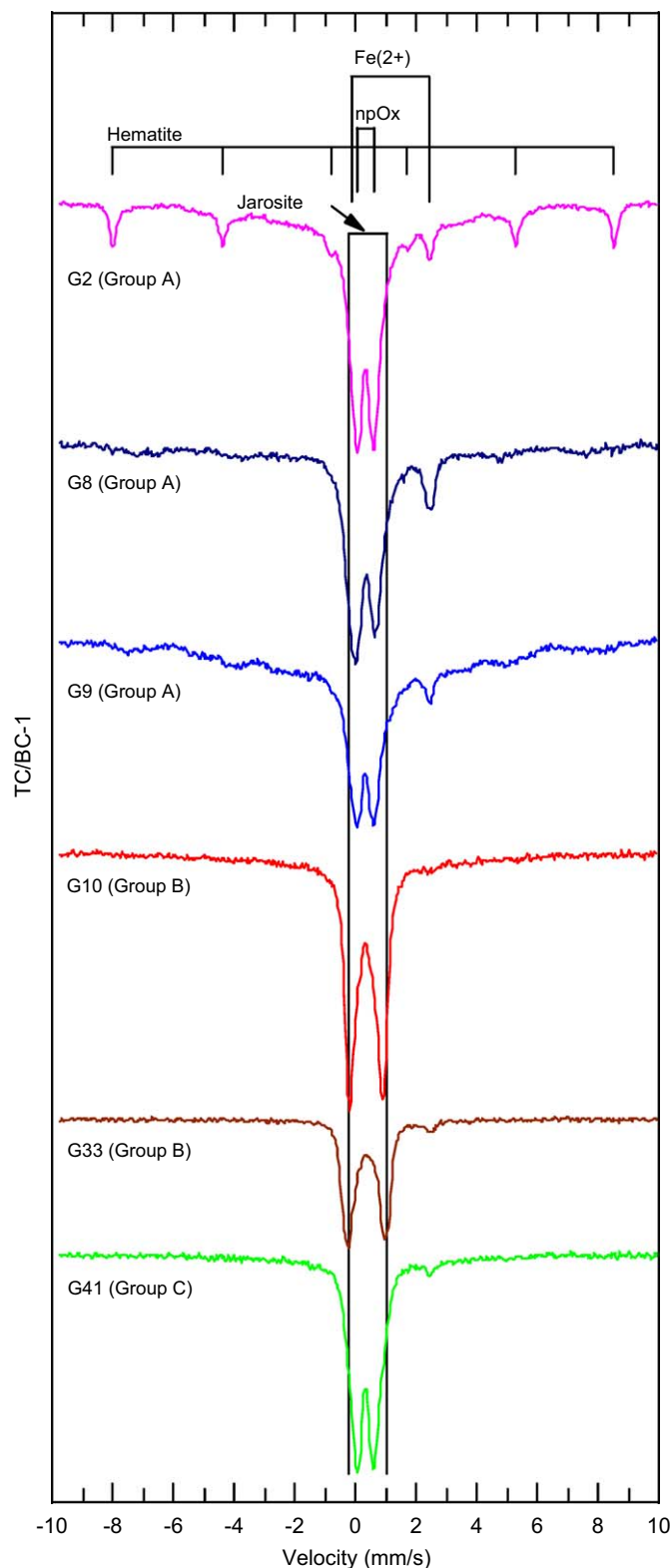


Fig. 5. Mössbauer spectra for High Lake gossan samples G2, G8 and G9 (Group A-site #1), for samples G10 and G33 (Group B-sites #1 and #2), and for sample G41 (Group C-site #3). Stick diagram indicates peak positions for subspectra from the Fe^{3+} -bearing phases hematite, jarosite, nanophase ferric oxide (npOx) and an unassigned Fe^{2+} -bearing phase. In addition, there is a broad contribution (most evident in G2 and G9), probably from one or more subspectra from partially relaxed sextet components. TC = total counts; BC = baseline counts.

G9 in Fig. 5) is consistent with small-particle (but not superparamagnetic) and/or substituted hematite, maghemite and/or magnetite. Similar forms of goethite can be

present, but would not have contributed to the high-velocity peaks.

NpOx is a generic name for an oct- Fe^{3+} alteration product, and the doublet can be any combination of ferrihydrite, schwertmannite, akaganeite, iddingsite, hisingerite, superparamagnetic hematite and goethite, and other poorly crystalline forms of oct- Fe^{3+} . NpOx was detected in all six samples analyzed by MB ($A = 11$ –94%), with G41 having the highest proportion of total Fe associated with npOx. Jarosite is detected by MB in samples G10 and G33 at high abundance ($A = 69\%$ and 82% , respectively). The hematite sextet was clearly present in sample G2 with $A = 12\%$.

The doublet from oct- Fe^{2+} was also detected in all MB samples ($A = 5\%$ –18%). The values of δ and ΔEQ were calculated from the sample with the highest contribution from the doublet (G8), and those values were used as fixed constraints in the other five samples. A possible (equivocal) mineralogical assignment for the oct- Fe^{2+} is clinocllore which was detected by XRD.

4. Discussion

4.1. Source rocks and setting

An important aspect of understanding the gossan mineral assemblages is the source rock mineral assemblage. Talc, anthophyllite and chlorites are all major metamorphic minerals in the High Lake metavolcanic sequences (Petch, 2005). Other important metamorphic minerals include quartz and muscovite, the latter of which might be the source of K and Al for sulfate minerals. Alternatively K feldspar in the felsic metavolcanic units might provide K and Al upon alteration. The Ca for gypsum formation could either arise from dissolution of abundant carbonate or plagioclase feldspar present in the volcanoclastic strata (Petch, 2005).

4.2. Phosphorus

Phosphorous appears in the SEM/EDS analyses, sometimes in relatively high amounts at High Lake and often in conjunction with Fe. Because of their generally small size ($<1\ \mu\text{m}$) and amorphous morphology, the diffraction lines from the Fe-phosphates in these samples are not present in the XRD patterns, but they are readily recognized under SEM/EDS.

Assuming apatite is the source mineral, the presence of P provides clues about the general geochemistry of the outcrops. Even at high HPO_4^{2-} concentrations, apatite is only stable in solutions with a pH greater than 6 (Dill, 2001). Its absence, therefore, implies a pore water pH that is less than 6. If apatite is the source, however, why is Ca not a common cation where PO_4^{3-} is an anion? The only real accumulation of Ca appears in the gypsum of sample G41. Geochemical modeling indicates that in the acidic solutions, Ca (as well as Na and Mg) phosphates are highly soluble and whereas Fe-phosphates, e.g. strengite, are not.

4.3. Geochemistry and evolution

The Group A samples contained predominantly npOX with hematite and minor goethite or ferrihydrite, rhomboclase and potentially schwertmannite being the only possible Fe-sulfates (Tables 1 and 2). Where this mineral assemblage has been observed in acid mine drainage (AMD) environments and the pH of the ambient water determined, the coexistence of goethite and schwertmannite suggests a pH of 3–5 (Murad and Rojik, 2005), whereas the presence of ferrihydrite indicates a pH of 5–8 (Murad

Table 2
Mössbauer parameters^a (293 K) for Fe-bearing phases for gossan samples from High Lake.

Sample	npOx			Jarosite			Fe ²⁺			Hematite				Broad ^b
	δ (mm/s)	Δ EQ (mm/s)	A (%)	δ (mm/s)	Δ EQ (mm/s)	A (%)	δ (mm/s)	Δ EQ (mm/s)	A (%)	δ (mm/s)	Δ EQ (mm/s)	B_{hf} (T)	A (%)	
G2	0.35 ^c	0.57 ^d	42 ^e	–	–	0	[1.13] ^f	[2.65]	5	0.37	–0.18	51.3 ^g	12	40 ^h
G8	[0.34]	[0.63]	64	–	–	0	1.13	2.65	18	–	–	–	0	18 ^h
G9	0.34	0.59	27	–	–	0	[1.13]	[2.65]	6	–	–	–	0	67 ^h
G10	[0.34]	[0.63]	28	0.36	1.12	69	[1.13]	[2.65]	3	–	–	–	0	0
G33	[0.34]	[0.63]	11	0.37	1.25	82	[1.13]	[2.65]	7	–	–	–	0	0
G41	0.35	0.62	94	–	–	0	[1.13]	[2.65]	6	–	–	–	0	0

^a δ = isomer shift relative to metallic Fe foil at 293 K; Δ EQ = quadrupole splitting; B_{hf} = hyperfine field strength; A = percentage of total Fe associated with Fe-bearing phase. Values of Γ for npOx, jarosite, and Fe²⁺ phase are 0.41–0.49, 0.35–0.39, and 0.34 mm/s, respectively.

^b Value of A for singlet subspectrum (δ = 0.34 mm/s and Γ = 4.0 mm/s) used to approximate the broad component.

^c Uncertainty in δ = ± 0.02 mm/s.

^d Uncertainty in Δ EQ = ± 0.02 mm/s.

^e Uncertainty in A = $\pm 2\%$ absolute unless otherwise specified.

^f MB parameters in brackets are constraints used in the least squares fitting procedure.

^g Uncertainty in B_{hf} = 0.8 T.

^h Uncertainty in A = $\pm 4\%$ absolute.

and Rojik, 2005). The presence of rhomboclase in G2, however, indicates that the pH was also much less (Dill, 2001). This range suggests that microenvironments with distinct pH values must exist in these samples, perhaps as a result of variable degrees of wetting during freeze/thaw cycles.

The SEM/EDS analyses revealed that G2, G8 and G9, and hence the gossan outcrop of site 1 (Fig. 1A), where these samples were collected, did not possess diverse sulfate-bearing phases, but rather contained a greater abundance of npOx than site #2. Other than the primary, metamorphic mineral, chlorite, Fe²⁺-bearing minerals were absent suggesting that any transformation of schwertmannite to goethite and ferrihydrite was complete and that any initial stage of Fe²⁺-sulfide oxidation resulting in the formation of Fe²⁺-sulfates, such as melanterite or siderotil, either did not occur or has since been altered. Continued exposure to the atmosphere would have oxidized Fe²⁺-sulfates into hydrated Fe²⁺/Fe³⁺ or Fe³⁺-sulfates that would finally hydrolyze into npOx, which is present in all samples (Table 2).

The predominant Fe-bearing mineral in Group B samples from site #2 is jarosite, which was seen frequently by SEM as cubic clusters throughout these samples (Fig. 4C). Jarosite, especially at the low water-to-rock ratio present in these soils, is stable at pH levels down to 0.5 (Fig. 6A). In the presence of PO₄³⁻ K-rich jarosite should only form in a narrow pH range slightly under 1 when the fO_2 is greater than 10^{-35} bars (Fig. 6A). The presence of jarosite also requires SO₄²⁻ concentrations > 3000 mg L⁻¹. Notably absent from any of the analyses was alunite [KAl₃(SO₄)₂(OH)₆]. This may be because it should only form where pH is between 3 and 4 whereas jarosite will form in solutions where the pH is < 3 . Jarosite is one of the last forming salt minerals at other AMD sites (Buckby et al., 2003). Although Majzlan and Myeni (2005) note that the formation of well-crystalline Fe³⁺ sulfates may require extended time and elevated temperatures, this does not seem to be the case at High Lake.

Sample G41 is a mixture of Fe-oxides, jarosite and gypsum with minor phosphate minerals. In this sample, jarosite is less common than in the Group B samples and is seen by SEM to be growing on top of all the other minerals including the fine-grained Fe-oxides. Geochemical modeling indicates that dehydration of a sulfate-bearing, acidic solution increases the pH from 1.5 to 2.8 (Fig. 6A) while precipitating jarosite and strengite and dissolving goethite (Fig. 6B). Such a situation could be occurring as the soils dry out after the melting of the snow layer at the end of spring or during a freezing cycle. The gypsum, meanwhile, should be a

stable mineral at any pH between 0 and 6.5 with a fO_2 greater than 10^{-70} .

4.4. Comparison of high lake to other AMD Sites and Meridiani Planum

The number of sulfate mineral species at the High Lake gossan is far fewer than has been reported at either Richmond Mine or Rio Tinto. More than 13 different sulfate minerals have been reported at Richmond Mine and 20 at Rio Tinto (Buckby et al., 2003), whereas, only gypsum, jarosite, rhomboclase, yavapaiite and possibly schwertmannite were detected at High Lake. Notably absent are any of the Fe²⁺ sulfates that are present at the other sites. One possibility is that lower sulfate concentrations combined with higher phosphate concentrations to limit the amount of Fe²⁺ sulfates that can be produced. The jarosite at High Lake is the Na and K bearing variety due to the abundance of the alkali metals in the host rock. This may account for its stability versus that of hydronium jarosite, which is the dominant jarosite phase at Rio Tinto.

The presence of Fe-phosphates is noteworthy. Fe-phosphates are known to occur in association with terrestrial gossans (Anthony et al., 2000) and in soils at Gusev Crater on Mars (Lane et al., 2007). However, substantial research involving Fe-phosphates has not been done (Lane et al., 2007), and they have not been reported at acid mine sites like Richmond Mine (Jamieson et al., 2004, 2005) or Rio Tinto (Fernandez-Remolar et al., 2003, 2005). Identifying and collecting better spectral data for the Fe-phosphates at High Lake could be an aim for future research.

The other difference between the High Lake gossan samples from those from the Rio Tinto and Richmond Mine is the smaller crystal sizes of the High Lake samples. Buckby et al. (2003) reported gypsum crystals that were over 50 μ m in size at Rio Tinto, whereas our SEM/EDS analyses revealed a maximum gypsum crystal size of 10 μ m. Jarosite at the Richmond Mine ranges between 2 and 5 μ m, whereas jarosite from High Lake is no larger than 1.5 μ m. This could be related to slower reactions rates at High Lake as a result of the lower temperatures and the short summer months when the ice cover is absent.

The mineral assemblages identified in the High Lake gossans bear a slight resemblance to those identified in Meridiani Planum by Opportunity. The sulfate-rich outcrop at Meridiani Planum, however, has a basaltic bulk chemical composition (normalized

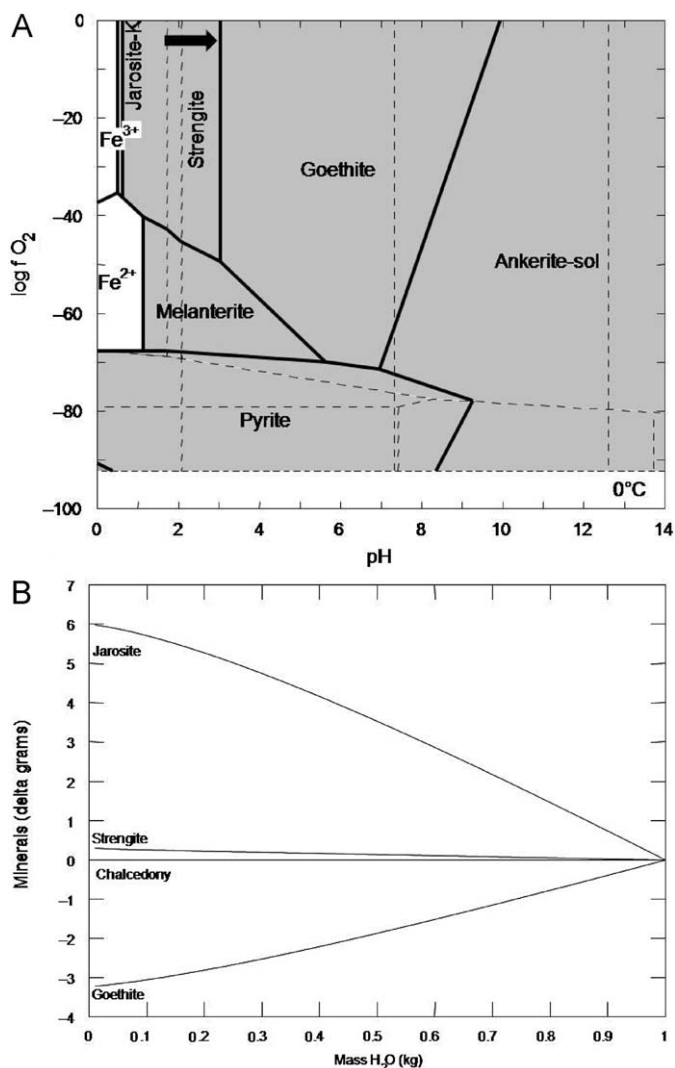


Fig. 6. (A) f_{O_2} versus pH diagram for Fe-S system. $p_{CO_2} = 10^{-3.5}$ bar; $a(SO_4^{2-}) = 10^{-1}$; $a(Cl^-) = 1$; $a(Na^+) = 1$; $a(K^+) = 10^{-1}$; $a(Mg^{2+}) = 10^{-1}$; $a(Ca^{2+}) = 10^{-1}$; $a(Fe^{2+}) = 10^{-1.5}$ and $a(HPO_4^{2-}) = 10^{-3}$. Solid lines demarcate Fe mineral phase boundaries. Dashed lines demarcate the sulfur species stability fields. Black arrow delineates change in pH during removal of 99% H_2O in reaction simulation. (B) Mineral precipitation and dissolution during removal of 99% H_2O in reaction simulation.

to a SO_3 -free basis), whereas High Lake is dominated by quartz-bearing, felsic metavolcanic and metavolcaniclastic sequence (Petch, 2005). The most Fe-enriched High Lake gossan sample, G2, does contain hematite, whereas samples of the metavolcanic rock do not, indicating that the hematite formed at low temperature, but not as spherical concretions. In sample G41, jarosite and fine-grained Fe-oxide were present, but hematite was not detected. In Meridiani Planum, jarosite and hematite are found in the same outcrop.

5. Conclusions

Samples from the gossan at High Lake were classified into two major assemblages. Group A was a Fe-oxide rich assemblage with Fe-oxides, chlorite, quartz and phosphates. Group B was comprised primarily of quartz, muscovite and jarosite. Group C was transitional between A and B and was represented by just one sample, G41, which contained a mixture of Fe-oxides, jarosite and gypsum.

The gossan mineral assemblages indicate that the solution geochemistry for mineral precipitation ranges from highly acidic and sulfate-rich (pH 0.5–3; $SO_4 > 3000 \text{ mg L}^{-1}$) for the Group B assemblage to mildly acidic, less sulfate-rich (pH 3–6; $SO_4 < 1000 \text{ mg L}^{-1}$) for the Group A assemblage. Both groups contained mainly Fe^{3+} minerals representing the later stages of oxidation and gossan development. Sample G41 appears to be in a transition zone from Fe-oxides into a jarosite-dominated assemblage, which may result from evaporation or freezing of the melt water leading to an increase in molality of sulfate and a decrease in pH.

Although the amount of phosphorus is surprising when compared to other AMD sites, all of the minerals are plausible derivatives from the sulfide-rich, metavolcanic rock on which the gossan has formed. The other differences between High Lake and the other AMD sites are the lack of diverse sulfate species and the smaller crystal size. The difference in sulfate species could arise from melting of the snow cap during the spring dissolving sulfate mineral species that formed during the remainder of the year. The smaller oxide, sulfate and phosphate crystal sizes, meanwhile, may reflect the slower reaction rates in the colder environment. The High Lake gossan demonstrates that hematite and jarosite, minerals that have been identified at Meridiani Planum, can form in an environment not related to evaporitic basins and one that is perpetually frozen for a majority of the year. The absence of hematite spherules may lead credence to their hypothesized high-temperature origin. To determine in greater detail, the relationships between the mineral assemblages and their environment will require determination of the pore water chemistry when the gossan is wetted by spring melt followed by evaporation during the summer and fall. The role played by microorganisms in the formation of these assemblages and whether they leave behind distinct biosignatures remains to be explored.

Acknowledgements

This work was supported by the NASA Astrobiology Institute through award NNA04CC03A to the IPTAI Team co-directed by LMP and TCO. We are indebted to Wolfden Resources Ltd. and Zinfex Canada Inc., Ian Neill, Jason Rickard, Patricia Toole and the staff of High Lake mining camp for providing logistical and moral support. We thank Peggy Bisher of the Molecular Biology Department at Princeton University for assistance with coating the samples for SEM analyses. We thank Jane Woodruff of the Princeton Materials Institute for assistance with SEM/EDS analyses. RVM acknowledges support of the NASA Mars Exploration Rover Project and the NASA Johnson Space Center.

References

- Anthony, J.W., Bideaux, R.A., Bladh, K.W., Nichols, M.C., 2000. Diadochite. In: Handbook of Mineralogy, Vol. 4. Mineral Data Publishing.
- Bethke, C.M., 1998. The Geochemist's Workbench Users Guide. University of Illinois, Champaign, Illinois.
- Bibring, J.-P., Langevin, Y., Gendrin, A., Gondet, B., Poulet, F., Berthe, M., Soufflot, A., Arvidson, R., Mangold, N., Mustard, J., Drossart, P., Team, a.t.O., 2005. Mars surface diversity as revealed by the OMEGA/Mars express observations. *Science* 307, 1576–1581.
- Buckby, T., Black, S., Coleman, M.L., Hodson, M.E., 2003. Fe-sulphate-rich evaporative mineral precipitates from the Rio Tinto, southwest Spain. *Mineralogical Magazine* 67, 263–278.
- Burns, R.G., 1988. Gossans on Mars. In: the Proceedings of the 18th Lunar and Planetary Science, pp. 713–721.
- Burns, R.G., Solberg, T.C., 1990. ^{57}Fe -bearing oxide, Silicate, and Aluminosilicate minerals, crystal structure trends in Mössbauer spectra. In: Spectroscopic Characterization of Minerals and Their Surfaces. American Chemical Society.
- Burt, D.M., Wohletz, K.H., Knauth, L.P., 2006. Mars and mine dumps. *EOS* 87, 549–552.
- Catling, D., 2004. On Earth, as it is on Mars? *Nature* 429, 707–708.

- Clark, B.C., Baird, A.K., Rose Jr., H.J., Toulmin III, P., Keil, K., Castro, A.J., Kelliher, W.C., Rowe, C.D., Evans, P.H., 1976. Inorganic analyses of martian surface samples at the Viking landing sites. *Science* 194, 1283–1288.
- Clark, B.C., 1993. Geochemical components in Martian soil. *Geochimica et Cosmochimica Acta* 57, 4574–4581.
- Dill, 2001. The geology of aluminum phosphates and sulphates of the alunite group minerals: a review. *Earth-Science Reviews* 53, 35–93.
- Fernandez-Remolar, D., Morris, R.V., Gruener, J.E., Amils, R., Knoll, A.H., 2005. The Rio Tinto Basin, Spain: mineralogy, sedimentary geobiology, and implications for interpretation of outcrop rocks at Meridiani Planum, Mars. *Earth and Planetary Science Letters* 240, 149–167.
- Fernandez-Remolar, D.C., Rodriguez, N., Gomez, F., 2003. Geological record of an acidic environment driven by iron hydrochemistry: the Tinto river system. *Journal of Geophysical Research* 108, 1–16.
- Golden, D.C., Ming, D.W., Morris, R.V., Graff, T.G., 2008. Hydrothermal synthesis of hematite spherules and jarosite: implications for diagenesis and hematite spherule formation in sulfate outcrops at Meridiani Planum, Mars. *American Mineralogist* 93, 1201–1214.
- Grotzinger, J., Bell III, J., Herkenhoff, K., Johnson, J., Knoll, A., McCartney, E., McLennan, S., Metz, J., Moore, J., Squyres, S., Sullivan, R., Ahronson, O., Arvidson, R., Jolliff, B., Golombek, M., Lewis, K., Parker, T., Soderblom, J., 2006. Sedimentary textures formed by aqueous processes, Erebus crater, Meridiani Planum, Mars. *Geological Society of America* 34, 1085–1088.
- Grotzinger, J.P., Arvidson, R.E., Bell III, J.F., Calvin, W., Clark, B.C., Fike, D.A., Golombek, M., Greeley, R., Haldemann, A., Herkenhoff, K.E., Jolliff, B.L., Knoll, A.H., Malin, M., McLennan, S.M., Parker, T., Soderblom, L., Sohl-Dickstein, J.N., Squyres, S.W., Tosca, N.J., Watters, W.A., 2005. Stratigraphy and sedimentology of a dry to wet eolian depositional system, Burns formation, Meridiani Planum, Mars. *Earth and Planetary Science Letters* 240, 11–72.
- Jamieson, H.E., Robinson, C., Alpers, C.N., McCleskey, R.B., Nordstrom, D.K., Peterson, R.C., 2004. Major and trace element composition of copiapite-group minerals and coexisting water from the Richmond mine, Iron Mountain, California. *Chemical Geology* 215, 387–405.
- Jamieson, H.H., Robinson, C., Alpers, C.N., Nordstrom, D.K., Poustovetov, A., Lowers, H.A., 2005. The composition of coexisting jarosite-group minerals and water from the Richmond Mine, Iron Mountain, California. *The Canadian Mineralogist* 43, 1225–1242.
- Klingelhöfer, G., Morris, R.V., Bernhardt, B., Schröder, C., Rodionov, D.S., de Souza Jr., P.A., Yen, A., Gellert, R., Evlanov, E.N., Zubkov, B., Foh, J., Bonnes, U., Kankeleit, E., Gutlich, P., Ming, D.W., Renz, F., Wdowiak, T., Squyres, S.W., Arvidson, R.E., 2004. Jarosite and hematite at Meridiani Planum from Opportunity's Mössbauer spectrometer. *Science* 306, 1740–1745.
- Knauth, L.P., Burt, D.M., Wohletz, K.H., 2005. Impact origin of sediments at the opportunity landing site on Mars. *Nature* 438, 1123–1128.
- Lane, M.D., Bishop, J.L., Dyar, M.D., Parente, M., King, P.L., Hyde, B.C., 2007. Identifying the phosphate and ferric sulfate minerals in the Paso Robles soils (Gusev Crater, Mars) using an integrated spectral approach. *Lunar and Planetary Science XXXVIII*, 2176.
- Langevin, Y., Poulet, F., Bibring, J.-P., Gondet, B., 2005. Sulfates in the north polar region of Mars detected by OMEGA/Mars express. *Science* 307, 1584–1586.
- Majzlan, J., Myeni, S., 2005. Speciation of iron and sulfate in acid waters: aqueous clusters to mineral precipitates. *Environmental Science & Technology* 39, 188–194.
- McCammom, C., 1995. Mössbauer spectroscopy of minerals. In: Ahrens, T.J. (Ed.), *Mineral Physics and Crystallography: A Handbook of Physical Constants*. American Geophysical Union.
- McCullom, T.M., Hynek, B., 2005. A volcanic environment for bedrock diagenesis at Meridiani Planum on Mars. *Nature* 438, 1129–1131.
- McLennan, S.M., Bell III, J.F., Calvin, W.M., Christensen, P.R., Clark, B.C., Souza, P.A., Farmer, J., Farrand, W.H., Fike, D.A., Gellert, R., Ghosh, A., Glotch, T.D., Grotzinger, J.P., Hahn, B., Herkenhoff, K.E., Hurowitz, J.A., Johnson, J.R., Johnson, S.S., Jolliff, B., fer, G.K., Knoll, A.H., Learner, Z., Malin, M.C., Mc Sween Jr., H.Y., Pockock, J., Ruff, S.W., Soderblom, L.A., Squyres, S.W., Tosca, N.J., Watters, W.A., Wyatt, M.B., Yen, A., 2005. Provenance and diagenesis of the evaporite-bearing Burns formation, Meridiani Planum, Mars. *Earth and Planetary Science Letters* 240, 95–121.
- Morris, R.V., Golden, D.C., Bell III, J.F., Shelper, T.D., Scheinost, A.C., Hinman, N.W., Furniss, G., Mertzman, S.A., Bishop, J.L., Ming, D.W., Allen, C.C., Britt, D.T., 2000. Mineralogy, composition, and alteration of Mars Pathfinder rocks and soils: evidence from multispectral, elemental, and magnetic data on terrestrial analogue, SNC meteorite, and Pathfinder samples. *Journal of Geophysical Research* 105, 1757–1817.
- Morris, R.V., Ming, D.W., Graff, T.G., Arvidson, R.E., Bell III, J.F., Squyres, S.W., Mertzman, S.A., Gruener, J.E., Golden, D.C., Le, L., Robinson, G.A., 2005. Hematite spherules in basaltic tephra altered under aqueous, acid-sulfate conditions on Mauna Kea volcano, Hawaii: possible clues for the occurrence of hematite-rich spherules in the Burns formation at Meridiani Planum, Mars. *Earth and Planetary Science Letters* 240, 168–178.
- Morris, R.V., Klingelhöfer, G., Schröder, C., Rodionov, D.S., Yen, A., Ming, D.W., de Souza Jr., P.A., Fleischer, I., Wdowiak, T., Gellert, R., Bernhardt, B., Bonnes, U., Cohen, B.A., Evlanov, E.N., Foh, J., Gütlich, P., Kankeleit, E., McCoy, T., Mittlefehldt, D.W., Renz, F., Schmidt, M.E., Zubkov, B., Squyres, S.W., Arvidson, R.E., 2006. Mössbauer mineralogy of rock, soil, and dust at Meridiani Planum, Mars: opportunity's journey across sulfate-rich outcrop, basaltic sand and dust, and hematite lag deposits. *Journal of Geophysical Research* 111, E12515.
- Murad, E., Rokj, P., 2005. Iron mineralogy of mine-drainage precipitates as environmental indicators; review of current concepts and a case study from the Sokolov Basin, Czech Republic. *Clay Minerals* 40, 427–440.
- Petch, C.A., 2005. The geology and mineralization of the high lake volcanic-hosted massive sulfide deposit, nunavut. *Exploration and Mining Geology* 13, 37–47.
- Pfiffner, S.M., Onstott, T.C., Ruskeeniemi, T., Talikka, M., Bakermans, C., McGown, D., Chan, E., Johnson, A., Phelps, T.J., Le Puil, M., Difurio, S.A., Pratt, L.M., Stotler, R., Frap, S., Telling, J., Sherwood-Lollar, B., Neill, I., Zerin, B., 2008. Challenges for Coring Deep Permafrost on Earth and Mars. *Astrobiology Journal* 8, 623–638.
- Rieder, R., Gellert, R., Anderson, R.C., Breuchner, J., Clark, B.C., Dreibus, G., Economou, T., Klingelhöfer, G., Lugmair, G.W., Ming, D.W., d'Uston, C., Waenke, H., Yen, A., Zipfel, J., 2004. Chemistry of rocks and soils at Meridiani Planum from the alpha particle X-ray Spectrometer. *Science* 306, 1746–1749.
- Salkield, L., 1987. A technical history of the Rio Tinto mines: some notes on exploitation from pre-phoenician times to the 1950s. In: Cahalan, M.J. (Ed.), *London Institution of Mining and Metallurgy*. Elsevier Science Ltd.
- Schiffman, P., Zierenberg, R., Marks, N., Bishop, J.L., Dyar, M.D., 2006. Acid-fog deposition at Kiluaea volcano: a possible mechanism for the formation of siliceous-sulfate rock coatings on Mars. *Geology* 34, 921–924.
- Stevens, J.G., Khasanov, A.M., Miller, J.W., Pollak, H., Li, Z., 1998. *Mössbauer Mineral Handbook*. Biltmore Press, Ashville, N.C.
- Squyres, S.W., Grotzinger, J.P., Arvidson, R.E., Bell III, J.F., Calvin, W., Christensen, P.R., Clark, B.C., Crisp, J.A., Farrand, W.H., Herkenhoff, K.E., Johnson, J.R., Klingelhöfer, G., Knoll, A.H., McLennan, S.M., McSween Jr., H.Y., Morris, R.V., Rice Jr., J.W., Rieder, R., Soderblom, L.A., 2004. In situ evidence for an ancient aqueous environment at Meridiani Planum, Mars. *Science* 306, 1709–1714.
- Zimbelman, D.R., Rye, R.O., Breit, G.N., 2004. Origin of secondary sulfate minerals on active andesitic stratovolcanoes. *Chemical Geology* 215, 37–60.